

Article

Using the Spatiotemporal Hot Spot Analysis and Multi-Annual Landslide Inventories to Analyze the Evolution and Characteristic of Rainfall-Induced Landslide at the Subwatershed Scale in Taiwan

Chunhung Wu

Department of Water Resources Engineering and Conservation, Feng Chia University, Taichung 40724, Taiwan; chhuwu@fcu.edu.tw; Tel.: +886-4-24517250-3231

Abstract: This study used rainfall and annual landslide data for the 2003–2017 period in Taiwan to determine the long-term evolution of landslides and conducted a spatiotemporal analysis of landslides at the subwatershed scale. The historically severe landslide induced by Typhoon Morakot in 2009 was mainly distributed in the central mountainous region and southern Taiwan. The Mann–Kendall trend test revealed that in 2003–2017, 13.2% of subwatersheds in Taiwan exhibited an upward trend of landslide evolution. Local outlier analysis results revealed that the landslide high–high cluster was concentrated in the central mountainous region and southern Taiwan. Moreover, the spatiotemporal analysis indicated 24.2% of subwatersheds in Taiwan in 2003–2017 as spatiotemporal landslide hot spots. The main patterns of spatiotemporal landslide hot spots in 2003–2017 were consecutive, intensifying, persistent, oscillating, and sporadic hot spots. The recovery rate in the first two years after the extreme rainfall-induced landslide event in Taiwan was 22.2%, and that in the third to eighth years was 31.6%. The recovery rate after extreme rainfall-induced landslides in Taiwan was higher than that after major earthquake-induced landslides in the world, and the new landslides were easily induced in the area of rivers and large landslide cases after Typhoon Morakot in 2009.

Keywords: landslide evolution; landslide recovery rate; local outlier analysis; Mann–Kendall trend test; spatiotemporal analysis; sub-watershed scale; Taiwan



Citation: Wu, C. Using the Spatiotemporal Hot Spot Analysis and Multi-Annual Landslide Inventories to Analyze the Evolution and Characteristic of Rainfall-Induced Landslide at the Subwatershed Scale in Taiwan. *Water* **2023**, *15*, 1355. <https://doi.org/10.3390/w15071355>

Academic Editor: Su-Chin Chen

Received: 23 February 2023

Revised: 25 March 2023

Accepted: 28 March 2023

Published: 1 April 2023



Copyright: © 2023 by the author. Licensee MDPI, Basel, Switzerland. This article is an open access article distributed under the terms and conditions of the Creative Commons Attribution (CC BY) license (<https://creativecommons.org/licenses/by/4.0/>).

1. Introduction

The rainfall variability under the present and future climate is examined as a function of global warming [1]. The trend of extreme rainfall events has been rising during the last three decades [2], and flood events are sensitive to global climate changes [3]. Rainfall-induced landslides are a common geological disaster in Taiwan that jeopardizes the safety of human life and property. The most severe rainfall-induced landslide disasters have been recorded in Taiwan in the past three decades, especially in 2001–2010 [4–7]. During 2001–2010, deaths caused by landslide disasters in Taiwan exceeded 1000, including 214 in 2001 caused by Typhoon Toraji, 45 in 2004 caused by Typhoon Mindulle, 33 in 2004 caused by Typhoon Aere, 21 in 2008 caused by Typhoon Sinlaku, and 699 in 2009 caused by Typhoon Morakot. Debris flow and sediment deposition in rivers are secondary geological disasters in watershed units caused by extreme rainfall-induced landslides [8,9]. The dense distribution of landslides and high sediment deposition in rivers have been the two main driving forces for the long-term geomorphologic evolution of landslides in mountainous watersheds in Taiwan in the past decade. Strategies for predicting landslides based on the characteristics of long-term landslide evolution must be developed to mitigate the effects of landslide disasters and secondary geological disasters.

Landslides caused by large-scale earthquakes or extreme rainfall events are usually clustered in mountainous areas near the earthquake epicenter [10–12] or with abundant rainfall during extreme rainfall events [6,13]. The spatial-temporal analysis method has been

widely used to explore the long-term evolution and distribution of specific phenomena, including water use efficiency [14], the long-term GDP development trend [15], groundwater storage [16], observation of crop growth [17], and urban sprawl [18]. To effectively analyze the temporal distribution and evolution of landslides, a spatiotemporal landslide database should be developed by combining multitemporal landslide inventories [8]. Multitemporal high-resolution and NDVI satellite imagery has been used to build multitemporal landslide inventories for identifying and analyzing multiple landslides [10,19,20]. Satellite images captured by FORMOSAT-2 with a spatial resolution of 2 m during 2003–2017 were used to develop annual landslide inventories in Taiwan. Several serious landslide disaster events occurred during 2003–2017 in Taiwan [21,22]. The spatiotemporal landslide database can be used to analyze the long-term evolution, distribution, and characteristics of landslides in Taiwan [8,9,23].

Landslide evolution analysis has been used to observe the long-term deformation of specific large landslide cases [24,25] or the spatial and temporal distribution of landslides on a watershed scale [8,10–12]. Long-term landslide evolution analysis needs multi-temporal remote sensing data, including SPOT images, interferometric synthetic aperture radar (InSAR), and light detection and ranging (LIDAR), to produce landslide inventories, NDVI images, or a digital elevation model for deformation observation [8–12,19–21,26–31]. The long-term evolution of landslides on a watershed scale has been increasingly studied in the past decade, especially in areas that experience major earthquake events (2005 Kashmir earthquake in Pakistan, 2008 Wenchuan earthquake in China, and 2015 Gorkha earthquake in Nepal) or extreme rainfall events (2009 Typhoon Morakot in southern Taiwan). Many approaches have been used to analyze the long-term evolution of landslides, including the evaluation of the spatial and temporal distribution of landslides using annual data of landslide areas and the number of landslides [10,11,19,26,27], evaluation of the spatial distribution of new, enlarged, and recovered landslides [19,26,27], assessment of the relationship between the spatial distribution of annual landslides and geomorphological factors [10,11,19,26,28], and assessment of the spatial and temporal distribution of landslide activity [10,11,19,26]. The temporal stability of landslides at the subwatershed scale has been examined by evaluating the relationship between annual rainfall [17], monthly rainfall [10], or daily rainfall [19] and the annual number of landslides or area of landslides. Images taken at multiple time points, including those obtained from Google Earth, aerial photographs, and field investigation images, have also been used to study temporal differences in landslide stability and recovery [19,20,26]. The landslide area frequency distribution have been used to examine the composition of recurring and new landslide areas in landslide inventories [20], and the β coefficient of the landslide area frequency distribution was used as a basis for comparison with other earthquake-induced landslide events [28].

The analysis of landslide evolution usually requires more than 10 years of climate data and landslide inventories [5,27]. In this study, we used the hot spot analysis tool to evaluate the characteristics of long-term landslide evolution and distribution in Taiwan [32]. Typhoon Morakot induced the most severe rainfall-induced landslide events in the last two decades in Taiwan, especially in southern Taiwan. Taiwan is one of the most landslide-prone regions in the world [33], and the number of landslides and areas affected in Taiwan reached a historical peak during 1999–2017. The analysis of the long-term evolution of landslides in Taiwan at the subwatershed scale should help determine the evolution characteristics of rainfall-induced landslides.

The purpose of this study was to explore and explain the long-term evolution characteristics of rainfall-induced landslides at the subwatershed scale in Taiwan using annual landslide inventories from 2003 to 2017 and spatiotemporal hot spot technology. Knowing the long-term evolution characteristic of landslides can contribute to planning the correct engineering in the correct place to prevent secondary geological hazards, especially in a watershed with dense landslide distribution. The long-term rainfall records from 16 rainfall stations for the period 2003–2017 were collected, and the relationship between rainfall and

landslide evolution was analyzed. Two spatiotemporal landslide cube models were developed in this study. The first was based on the annual landslide inventories from 2003–2017 and was used for exploring the long-term evolution of landslides in Taiwan. The other model was based on the annual landslide inventories from 2008–2017 and used to explore the long-term evolution of landslides caused by Typhoon Morakot in 2009. Moreover, the complete set of hot spots was statistically analyzed. We used spatial cluster and outlier analysis to explore the spatial and temporal distribution of landslides in Taiwan and the emerging hot spot analysis tool to explore the spatial and temporal hot spot patterns of landslides in Taiwan. We also determined the spatial and temporal distribution of landslide recovery after extreme rainfall-induced landslide events and compared it with that after major earthquake-induced landslide events.

2. Study Area

The research area, Taiwan, is located in East Asia. The elevation in Taiwan ranges from 0 m to 3952 m, and the average elevation is around 738 m (Figure 1a). The slope in Taiwan ranges from 0° to 89.8° , and the average slope is around 21.8° . The area with a slope $>30^{\circ}$ occupies 38.3% of the total area in Taiwan. Based on the delineation of sub-watersheds proposed by the Soil and Water Conservation Bureau in 2021 [34], there were 839 sub-watersheds in Taiwan (Figure 1b). The average slope of the 839 sub-watersheds is 22.5° , and 42.1% of the 839 sub-watersheds have a slope $>30^{\circ}$.

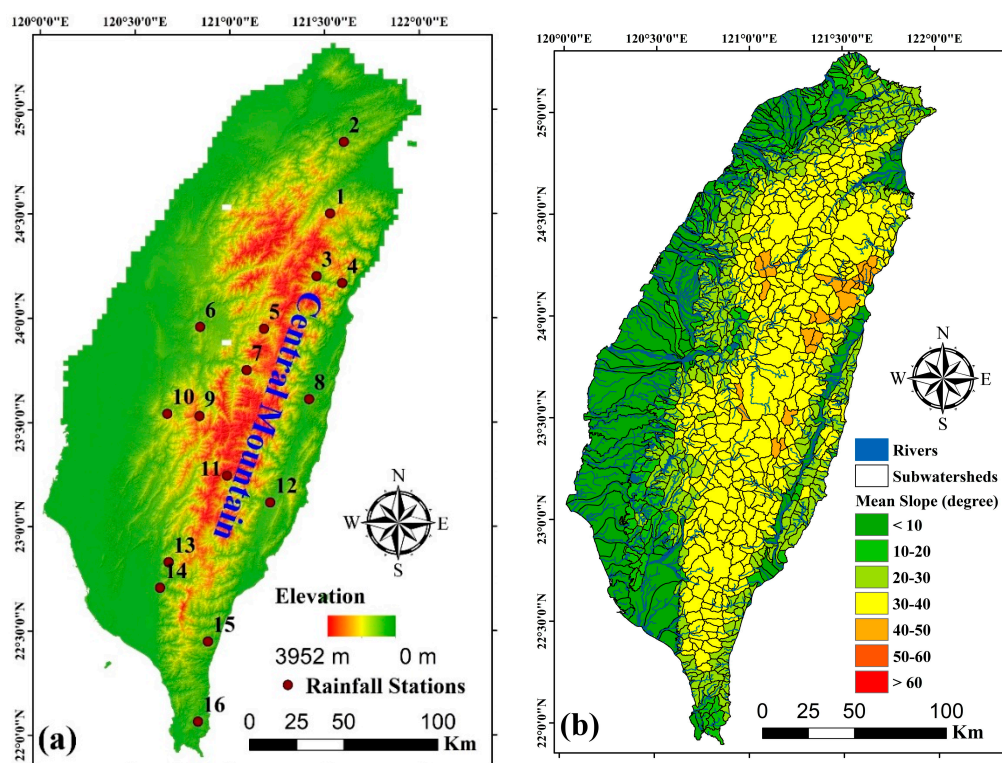


Figure 1. Distribution of elevation, rainfall stations (a), slope, rivers, and sub-watersheds (b) in Taiwan.

The long-term average annual rainfall in Taiwan was estimated at 2510 mm, but that in 2013–2020 was estimated at 2454 mm based on the open data information on the Water Resources Agency website [35]. The characteristic of annual rainfall in the past 2 decades in Taiwan was obvious oscillating. The average annual rainfall in 2014 and 2016 in Taiwan was 1921 mm and 3278 mm, and the difference between the annual rainfall in 2014 and 2016 was 1357 mm, i.e., 54.0% of the long-term average annual rainfall. The geological settings in Taiwan are shown in Figure 2. The terrace deposits (21.7%), alluvium (8.8%), and

Sanhsia group and its equivalents (7.7%) were the three main geological settings in Taiwan. The main stratigraphical formations in the northern central mountain region include the Oligocene-era Aoti formation, Oligocene-era Kankou formation, Eocene-era Szeleng sandstone, and Oligocene-era Tatungshan formation, and those in the southern central mountain region include Eocene-era Hsitsun Formation, Hsinkao Formation, Miocene-era Lushan Formation, late Miocene-era Sanhsia group and its equivalents, and late Paleozoic-era Tananao schist. Most landslides were concentrated in central and southern Taiwan, especially in the five landslide-prone stratigraphical formations, including the Changchihkeng Formation, Chaochou Formation, Pilushan Formation, Lushan Formation, and Tayuling Formation. The occupied percentage of the five landslide-prone stratigraphical formations in Taiwan is <30%, but the landslide area within the five landslide-prone stratigraphical formations after 2009 Typhoon Morakot occupied >70% of the all landslide areas in Taiwan. The main composition in the five landslide-prone stratigraphical formations are sandstone, shale, and slate. Detailed information of geological settings in Taiwan is also shown in Supplementary Materials.

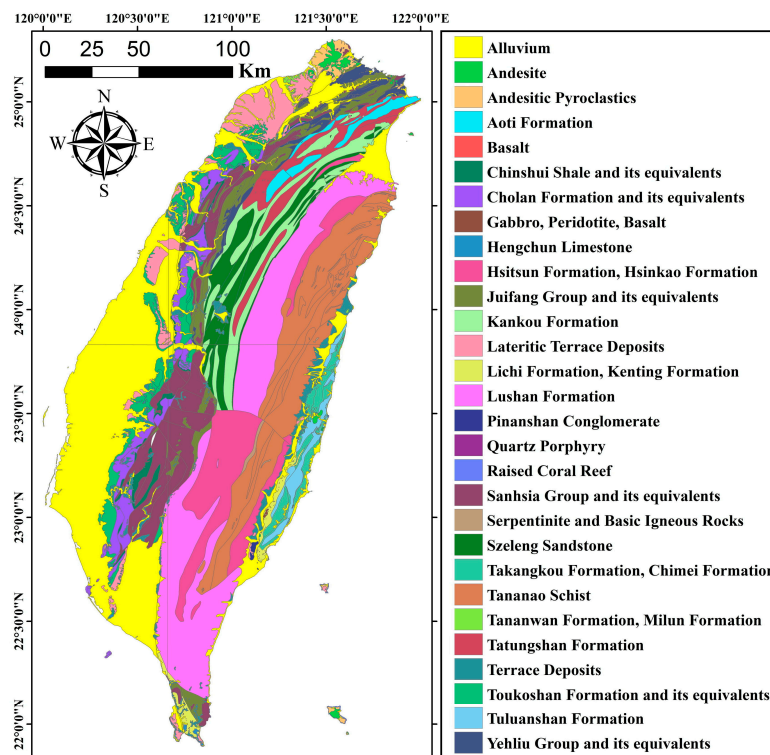


Figure 2. Geological settings in Taiwan (Scale 1:250,000).

3. Materials and Method

The flow chart of this research is shown in Figure 3.

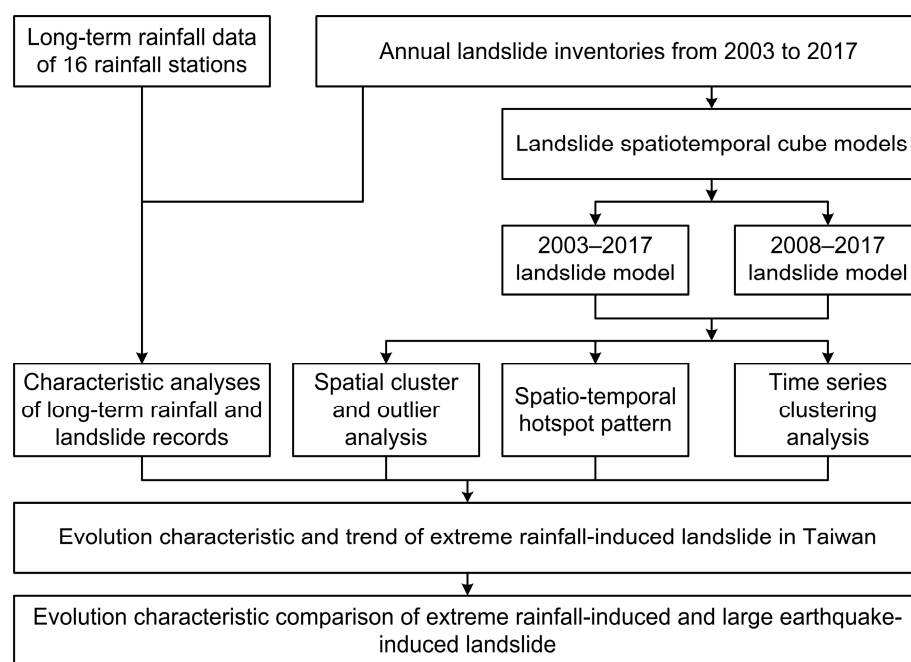


Figure 3. The flow chart in the study.

3.1. Materials

The rainfall data for the period 2003–2017 used in this study were collected from 16 rainfall stations (Figure 1a). Eight rainfall stations, namely stations 1, 3, 5, 7, 9, 11, 13, and 15, were located in the central mountainous region, which is the main spatiotemporal landslide hot spot in Taiwan, and the other eight rainfall stations, namely stations 2, 4, 6, 8, 10, 12, 14, and 16, were located outside the central mountainous region and not within the main spatiotemporal landslide hot spot. The data obtained from the 16 rainfall stations are detailed in the Supplementary Materials.

A digital elevation model with a resolution of 5 m was used in the study to conduct geomorphologic analyses. The delineation of subwatersheds in Taiwan (Figure 1b) was based on the proposed delineation from the Soil and Water Conservation Bureau [34], which is commonly used in research in Taiwan. The total area of 839 subwatersheds in Taiwan ranges from 0.39 to 575.8 km², with an average area of 42.9 km². Multiannual landslide inventories in 2003–2017 were generated by the Forestry Bureau in Taiwan by selecting images captured by the FORMOSAT-2 satellite with a spatial resolution of 2–5 m in January every year to identify landslides; this entails using a supervised classification method to develop landslide inventories for the previous year [18]. The production process of the annual distribution of landslides in 2003–2017 in Taiwan is shown in the Supplementary Materials. The large-scale landslide case considered in this study had a landslide area of >100,000 m².

3.2. Rainfall Seasonality Index (RSI)

Climatic factors are key to the recovery and long-term evolution of landslides, and the centralization of rainfall during the rainy seasons is a crucial factor that influences the recovery of rainfall-induced landslides in Taiwan [8,9,23]. The rainfall seasonality index (RSI) was used to measure the centralization of monthly rainfall in a year [36] and to assess the relationship between rainfall centralization and the recovery of earthquake-induced landslides in post-seismic periods [27]. The RSI is given [37] as follows:

$$RSI = \frac{1}{R} \sum_{n=1}^{12} \left| \bar{X}_n - \frac{\bar{R}}{12} \right| \quad (1)$$

where \bar{R} is the average annual rainfall in the research period and \bar{X}_n is the average monthly rainfall of the n th month in the research period. The centralization of monthly rainfall based on the RSI is described in Table 1 [38].

Table 1. The explanation of the centralization of monthly rainfall based on the rainfall seasonality index [36].

RSI	Rainfall Regime
≤ 0.19	Very equable
0.20–0.39	Equable but with a definite wetter season
0.40–0.59	Rather seasonal with a short drier season
0.60–0.79	Seasonal
0.80–0.99	Markedly seasonal with a long drier season
1.00–1.19	Most rain in 3 months or less
≥ 1.20	Extreme, almost rain in 1–2 months

Note: The table was reprinted with permission from Ref. [37]. 1981, Walsh, R.P.D. and Lawler, D.M.

3.3. Landslide Spatiotemporal Cube Models

The annual landslide inventories in 2003–2017 and 2008–2017 in Taiwan were used to construct the two spatiotemporal landslide cube models in this study, namely the 2003–2017 spatiotemporal landslide model and the 2008–2017 spatiotemporal landslide model. The 2003–2017 spatiotemporal landslide model was used to analyze the long-term evolution of landslides in Taiwan, and the 2008–2017 spatiotemporal landslide model was used to analyze the evolution of landslides caused by Typhoon Morakot. The basic unit in the spatiotemporal cube models was data from the 839 subwatersheds based in Taiwan. The x and y coordinates in the spatiotemporal cube model denote the x and y coordinates of the centroid in the subwatershed scale image and represent the spatial dimensions in a specific year. The term t denotes the time dimension. The landslide ratio in the subwatershed for a specific year was calculated using the spatiotemporal cube model and was defined as the ratio of the landslide area to the total subwatershed area. The process of building the spatiotemporal landslide cube models is shown in the Supplementary Materials. The spatiotemporal landslide cube models were developed using ArcGIS Pro software Ver 1.2, and the data were converted to the NetCDF data format. The spatiotemporal hot spot analyses were conducted using the NetCDF data set.

The Mann–Kendall test was used to measure the temporal trend of landslide ratio in a specific basic unit in the two spatiotemporal cube models. The temporal trend meant that the landslide ratio in a specific period had been increasing or decreasing over time. The purpose of the Mann–Kendall test was to compare the landslide ratio in the specific subwatershed between the current year and the previous year. A positive value, negative value, or value of 0 in the Mann–Kendall test indicated an increasing trend, a decreasing trend, or no obvious change, respectively, over time for the annual landslide distribution.

3.4. Spatial Cluster and Outlier Analysis

The spatial landslide pattern is key to identifying landslide-prone regions and determining landslide evolution. The Anselin Local Moran's I index [38] was used to explore the spatial clusters and outliers of landslides in space and time dimensions in the study. Based on the calculations obtained using the Anselin Local Moran's I index, the spatial landslide pattern can be classified into six types, including a statistically significant cluster of high values (only high–high cluster), a statistically significant cluster of low values (only low–low cluster), an outlier in which a high landslide ratio value was surrounded by low landslide ratio values (only high–low outlier), outlier in which a low landslide ratio value was surrounded by high landslide ratio values (only low–high outlier), multiple types, and never significant.

3.5. Spatiotemporal Hot Spot Patterns

Spatiotemporal hot spot patterns are useful in explaining landslide evolution and can be obtained by analyzing the spatiotemporal landslide cube models using the Space Time Pattern Mining toolbox in Arc GIS Pro software Ver 1.2. This tool can be used to analyze the distribution and patterns of multiannual landslide data in terms of both space and time. A basic unit in the spatiotemporal landslide cube model represents the landslide ratio in a specific subwatershed in a specific year, and all basic units were input into the emerging hot spot analysis tool. The statistically significant values of each basic unit were used to identify the types and spatiotemporal distribution of hot spots.

The hot spot analysis tool estimated the Getis-Ord G_i^* statistic for each basic unit in the spatiotemporal models [39]. The pattern of the spatiotemporal landslide hot spots was identified using the landslide ratio of the basic unit and the neighboring basic units in both space and time. If the landslide ratios exhibited high (low) significant clustering, the basic unit was identified as a hot (cold) spot. The statistical significance of each basic unit in the spatiotemporal landslide models was determined based on the z -scores and p values for the Getis-Ord G_i^* statistic [39]. If a basic unit had a high landslide ratio and was surrounded by other basic units with high landslide ratios, the basic unit was identified as a significant hot spot. Based on the z -score and p value of each basic unit in the spatiotemporal landslide model, eight patterns of hot and cold spots, or no pattern, were detected. The eight hot or cold spot patterns were new, consecutive, intensifying, persistent, diminishing, sporadic, oscillating, and historical. The original definition of 8 patterns had been described on the ESRI website [40], and the adjusted definition of 8 patterns which was suitable to characterize the pattern of landslide evolution is shown in Supplementary Materials. The new, consecutive, intensifying, persistent, diminishing, sporadic, oscillating, and historical hot spots were abbreviated as NHS, CHS, I, PHS, DHS, SHS, OHS, and HHS, respectively, in this study.

The 2003–2017 spatiotemporal landslide model contained 12,585 basic units, and the 2008–2017 spatiotemporal landslide model contained 8390 basic units. The spatial neighborhood distance and time step were set as 13.6–14.2 km and 5 years, respectively.

4. Results

4.1. Long-Term Spatial and Temporal Distribution of Rainfall and Landslide Data in 2003–2017

The annual rainfall distribution data for 2003–2017 were obtained from the 16 rainfall stations (Figure 1a) in Taiwan and are presented in Figure 4. The complete data obtained from the 16 rainfall stations are presented in the Supplementary Materials. The average annual rainfall in 2003–2017 (2993.3 mm) was slightly higher (by 56.9 mm) than that in 2008–2017 (2930.5 mm). The average annual rainfall at the eight rainfall stations in the central mountainous region in 2003–2017 (3158.7 mm) was slightly higher (by 330.8 mm) than that at the eight rainfall stations outside the central mountainous region (2827.9 mm). The average ratios of the accumulated rainfall in the rainy season (from May to October) to the annual rainfall in 2003–2017 at the eight rainfall stations inside and outside the central mountainous region were 79.0% and 80.7%, respectively. The data indicated that the average accumulated rainfall in the rainy season from 2003–2017 at the eight rainfall stations in the central mountainous region was higher by 213.3 mm than that at another eight rainfall stations outside the central mountainous region. The three largest differences in average annual rainfalls recorded in 2003–2017 between the rainfall stations in and outside the central mountainous region were 1803 mm (No. 11 and No. 12 rainfall stations located in southeastern Taiwan), 1172 mm (No. 13 and No. 14 rainfall stations located in southwestern Taiwan), and 464.3 mm (No. 1 and No. 2 rainfall stations located in northern Taiwan). The distribution of annual rainfall recorded at the 16 rainfall stations in 2003–2017 in Taiwan was oscillating, especially in southern Taiwan. The annual rainfall recorded at rainfall station No. 13 in 2005 and 2011 was 7012 and 1832 mm, respectively, and the difference in annual rainfall between 2005 and 2011 was 5180 mm, 1.21 times the average annual rainfall. Furthermore, the temporal distribution of rainfall in the central

mountainous region in southern Taiwan in 2003–2017 was obviously different from that outside the central mountainous region.

The annual number of landslides and their temporal distribution in 2003–2017 in Taiwan are shown in Figure 5. The annual landslide area in 2003–2017 in Taiwan ranged from 216.1 km² in 2008 to 623.1 km² in 2009, and the average annual landslide area was estimated to be 424.1 km². The average landslide ratio (i.e., the ratio of landslide area to total area) in Taiwan in 2003–2017 was 1.15%. Based on the analysis of landslides in Taiwan, areas with a landslide ratio of >1.0% can be considered areas with serious disaster occurrence [3]. The annual number of landslides in Taiwan ranged from 19,041 in 2008 to 51,898 in 2013, and the average annual number of landslides was estimated to be 32,070. The average landslide density in Taiwan in 2003–2017 was estimated to be 0.87/km². The annual number of large-scale landslides in 2003–2017 in Taiwan ranged from 279 in 2003 to 1036 in 2009, and the average number of large-scale landslides was estimated to be 638.5. Thus, for 2003–2017, Taiwan is regarded as a region with a serious disaster occurrence, especially for the period of 2009–2017.

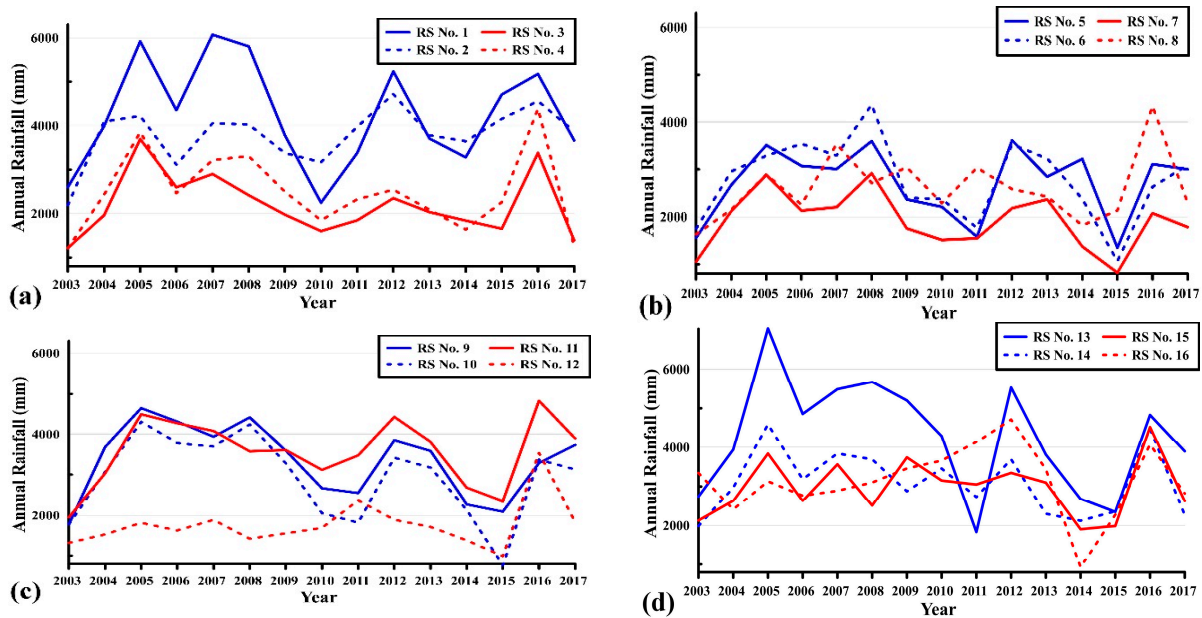


Figure 4. Temporal distribution of annual rainfall in the rainfall stations no. 1–4 (a), no. 5–8 (b), no. 9–12 (c), and no. 13–16 (d) in 2003–2017 in Taiwan.

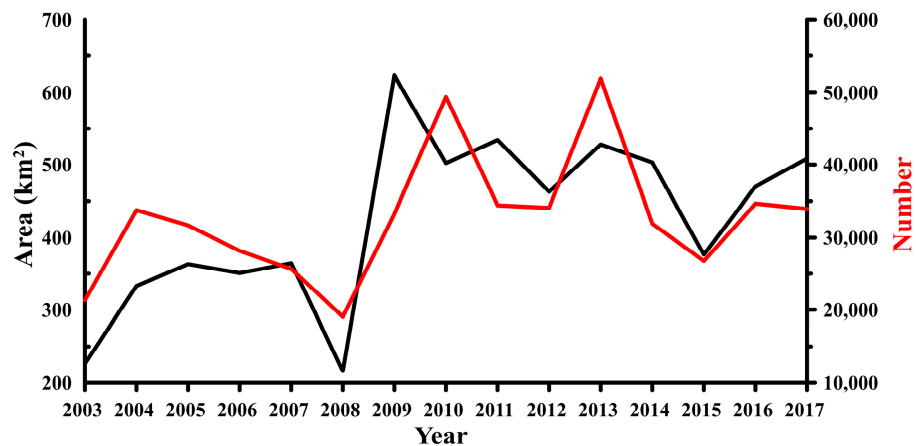


Figure 5. Temporal distribution of landslide area (black line) and number (red line) in 2003–2017 in Taiwan.

Taiwan has a nonuniform temporal distribution of annual and monthly rainfall, especially in southern Taiwan. The RSI was used to quantify the centralization of monthly rainfall at the 16 rainfall stations. Table 2 presents the average RSI values at the 16 rainfall stations in 2003–2017 in Taiwan. The rainfall stations located in the central mountainous region that recorded the top three highest RSI values were stations No. 13 (RSI = 0.78), No. 15 (RSI = 0.74), and No. 9 (RSI = 0.73). These three rainfall stations recorded relatively dry seasons (Table 1). High RSI values enable faster remobilization of sediment yield after severe landslide events [37]. The monthly rainfall regime in 2003–2017 in western, southwestern, and southern Taiwan exhibited obvious centralization, which implies that recovery after landslides in these three regions is more difficult and slower than in other regions in Taiwan.

Table 2. The rainfall seasonality index value in each region in Taiwan from 2003–2017.

No. of RS ¹	Region	RSI	No. of RS ¹	Region	RSI
1	Northern	0.62	9	Western	0.73
2	Taiwan	0.36	10	Taiwan	0.84
3	Eastern	0.47	11	Southeastern	0.76
4	Taiwan	0.65	12	Taiwan	0.70
5	Western	0.56	13	Southwestern	0.78
6	Taiwan	0.78	14	Taiwan	0.94
7	Eastern	0.64	15	Southern	0.74
8	Taiwan	0.45	16	Taiwan	0.64

Note: 1 means the number of rainfall stations in Figure 1a.

4.2. Landslide Spatialtemporal Cube Model and Trend

The 2003–2017 landslide model contained 12,585 basic units, and the 2008–2017 landslide model contained 8390 basic units. The results of the Mann–Kendall trend test for the two models are presented in Figure 6. In the 2003–2017 landslide model, 13.2%, 11.6%, and 75.2% of the subwatersheds accounted for upward, downward, and nonsignificant trends, respectively, whereas in the 2008–2017 landslide model, the corresponding percentages were 9.3%, 11.9%, and 78.8%, respectively. The subwatersheds exhibiting the upward trend in the 2003–2017 and 2008–2017 landslide models were concentrated in the central mountainous region of Taiwan, especially in southern Taiwan. This region was also severely affected by Typhoon Morakot. The subwatersheds exhibiting the downward trend in the 2003–2017 and 2008–2017 landslide models were spread across Taiwan and located outside the central mountainous region. The data indicated that the long-term evolution of landslides over 2003–2017 exhibited no obvious change after Typhoon Morakot in 2009, and that the landslide-prone subwatersheds were concentrated in the central mountainous region of Taiwan (i.e., upstream of the river watershed).

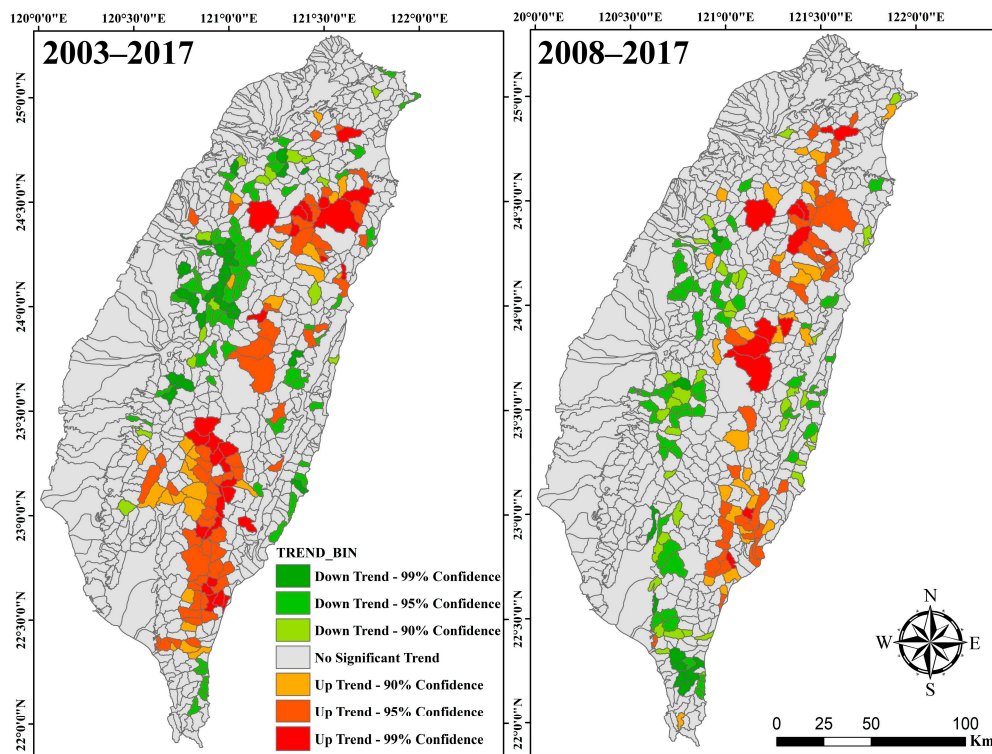


Figure 6. The Mann–Kendall trend test for the landslide cube model in 2003–2017 (left) and 2008–2017 (right).

4.3. Results of Spatial Clusters and Outliers

The distributions of the spatial landslide clusters and outliers in the 2003–2017 and 2008–2017 landslide models were analyzed using the local outlier analysis tool with a neighborhood time step of 5 years and 499 permutations in ArcGIS Pro software Ver 1.2. The results are shown in Figure 7. The high–high landslide cluster was still concentrated in the central mountainous region, whereas the low–low cluster was concentrated in the plains in west and north Taiwan. The statistical results of the spatial landslide cluster and outlier analyses are shown in Table 3.

A total of 447 and 502 subwatersheds were identified as significant spatial clusters (only high–high and only low–low) in the 2003–2017 and 2008–2017 landslide models, respectively. The only high–high cluster was distributed in the central mountainous region of south Taiwan in 2003–2017 and 2008–2017. This finding indicates that the central mountainous region in southern Taiwan was an originally landslide-prone region. The number of subwatersheds identified as having multiple types of patterns was 214 in 2003–2017 and decreased to 137 in 2008–2017; by contrast, the number of subwatersheds designated as never significant increased from 101 to 142, and the number designated as only the low–low cluster type increased from 241 to 305. The subwatersheds designated as multiple types in 2003–2017 and later identified as never significant, and only the low–low cluster type in 2008–2017 were mainly distributed in northern Taiwan. The number of subwatersheds designated as only the high–high cluster type in the 2008–2017 landslide model in north Taiwan was smaller than that in the 2003–2017 landslide model. This result indicated that the landslide recovery rate in northern Taiwan was gradually improving because the sediment deposition disaster caused by Typhoon Morakot was mainly distributed in southern Taiwan (see the annual landslide distribution in 2009–2017 in Supplementary Materials). The number of subwatersheds marked as only high–low outliers declined from 2003–2017 to 2008–2017, and these subwatersheds were mainly distributed in the piedmont regions across Taiwan. Only nine and five subwatersheds were

designated as only low–high outliers in the 2003–2017 and 2008–2017 landslide models, respectively, and these subwatersheds were mainly distributed in southern Taiwan.

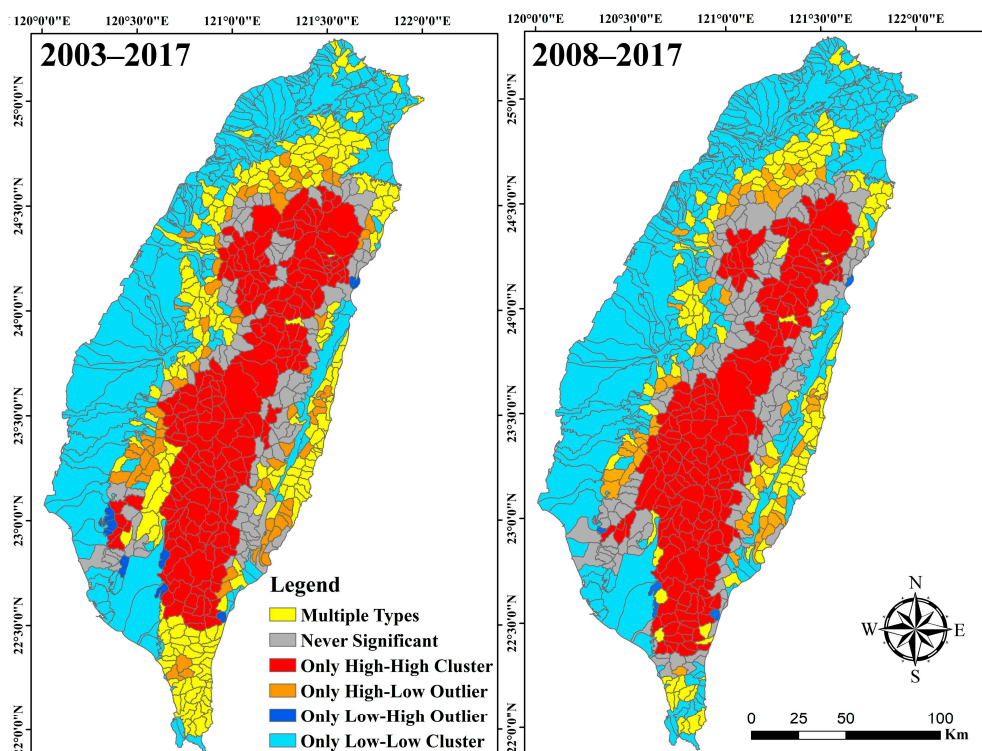


Figure 7. Distribution of landslide spatial cluster and outlier using the Anselin Local Moran’s I index.

Table 3. Statistical data of landslide spatial clusters and outlier analyses in Taiwan.

Type	Numbers of Sub-Watersheds	
	2003–2017	2008–2017
Mul. *	214	137
NS *	101	142
HH *	206	197
HL *	68	53
LH *	9	5
LL *	241	305

Note: * The Mul., NS, HH, HL, LH, and LL mean multiple, never significant, only high-high cluster, only high-low outlier, only low-high outlier, only low-low cluster types.

4.4. Landslide Spatiotemporal Hot Spot Analyses

The distribution and pattern of the spatiotemporal landslide hot spots in the 2003–2017 and 2008–2017 landslide models obtained using the emerging hot spot analysis tool in ArcGIS Pro software are shown in Figure 8. The statistical data of the spatiotemporal landslide hot and cold spots in Taiwan are presented in Table 4. The percentages of subwatersheds marked as hot spots in the 2003–2017 and 2008–2017 landslide models were 24.2% and 22.6%, and those of subwatersheds marked as cold spots were 50.1% and 52.8%. The landslide hot spots in the 2003–2017 and 2008–2017 landslide models were concentrated in the central mountainous region, but the pattern of spatiotemporal landslide hot spots in the 2003–2017 landslide model was obviously more concentrated than that in the 2008–2017 landslide model. The spatiotemporal hot spot pattern of subwatersheds accounting for >1.0% in the 2003–2017 landslide model included the consecutive hot spot (13.2%), intensifying hot spot (6.0%), persistent hot spot (1.8%), oscillating hot spot (1.5%),

and sporadic hot spot (1.0%), but the pattern in the 2008–2017 landslide model included only the consecutive hot spot (21.9%).

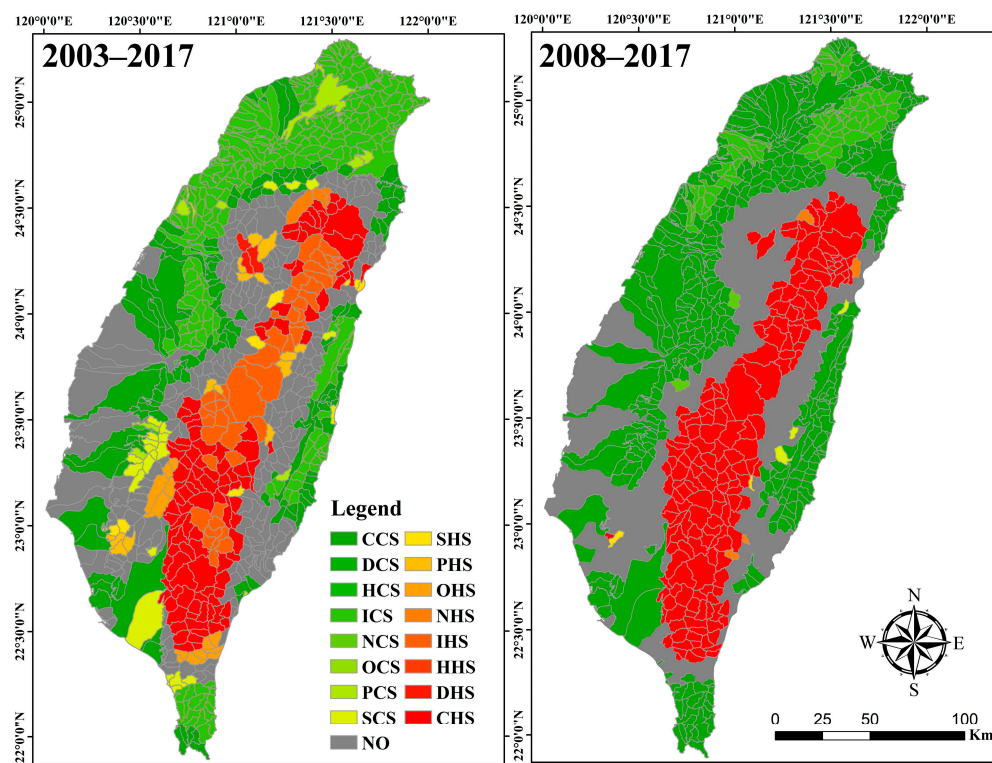


Figure 8. Distribution and pattern of landslide spatiotemporal hot spots in the 2003–2017 and 2008–2017 landslide models.

Table 4. Occupied percentage of landslide spatiotemporal hot spots and cold spots in 2003–2017 and 2008–2017 in Taiwan.

Pattern	Occupied Percentage		Pattern	Occupied Percentage	
	2003–2017	2008–2017		2003–2017	2008–2017
Cold spot	50.1	52.8	Hot spot	24.2	22.6
CCS	15.5	44.0	CHS	13.2	21.9
DCS	0.0	0.0	DHS	0.4	0.0
HCS	0.0	0.0	HHS	0.0	0.0
ICS	30.5	8.2	IHS	6.0	0.0
NCS	0.0	0.2	NHS	0.4	0.5
OCS	0.0	0.0	OHS	1.5	0.0
PCS	1.2	0.0	PHS	1.8	0.0
SCS	2.9	0.4	SHS	1.0	0.2
No pattern	25.7	24.6			

The trend and pattern of the distribution of landslide cold spots in the 2003–2017 and 2008–2017 models were similar to those of the distribution of landslide hot spots. The spatiotemporal cold spot pattern of subwatersheds accounting for >1.0% in the 2003–2017 landslide model included the intensifying cold spot (30.5%), consecutive cold spot (15.5%), sporadic cold spot (2.9%), and persistent cold spot (1.2%), but the pattern in the 2008–2017 landslide model only included the consecutive cold spot (44.0%) and intensifying cold spot (8.2%). The percentage of subwatersheds marked as having no pattern was 25.7% and 24.6%, respectively, in the 2003–2017 and 2008–2017 models. This result indicated that the spatiotemporal landslide hot spots were still primarily distributed in the central mountainous region of Taiwan.

5. Discussion

A comparison of the spatial and temporal distribution of landslide stability after severe landslide events induced by large-scale earthquakes and extreme rainfall can help clarify the characteristics of landslide recovery. Some studies [10,12,19,26] have elucidated the spatial and temporal distribution of landslide stability using the landslide recovery rate after large-scale earthquake-induced landslide events. The landslide recovery rate was defined as the ratio of the difference between the landslide area in a specific year and the landslide area in an earthquake-induced or rainfall-induced landslide year to the landslide area in an earthquake-induced or rainfall-induced landslide year. A comparison of the annual landslide recovery rate between earthquake-induced and extreme rainfall-induced landslide areas can reveal the characteristic differences between earthquake-induced and rainfall-induced landslide recovery.

The annual landslide recovery rate in northern Sichuan Province, China, in the first two years after the 2008 Wenchuan earthquake, was estimated to be 13.45%, and that in the third to eighth years was estimated to be 10.56% [41]. The landslide recovery rates in northern Pakistan in the fifth, ninth, eleventh, and thirteenth years after the 2005 Kashmir earthquake were 9.5%, 43.8%, 50.2%, and 61.3%, respectively [10]. Typhoon Morakot in 2009 was the most severe rainfall-induced landslide event during 2003–2017 in Taiwan. The number of landslides and the area affected in 2008 in Taiwan were estimated to be 19,041 and 167.1 km², respectively, and those in 2009 were estimated to be 33,274 and 502.2 km², respectively. The mean annual landslide ratio of 839 subwatersheds in 2009 in Taiwan was estimated to be 1.33%, and that in the first to second years and third to eighth years after Typhoon Morakot ranged from 1.01% to 1.06% and 0.71% to 1.01%, respectively. The landslide recovery rate in the first to second years after Typhoon Morakot in the 839 subwatersheds was estimated to be 22.2%, and that in the third to eighth years was estimated to be 31.6%.

The landslide recovery rate in the landslide-affected subwatersheds in the study was estimated to assess the actual landslide recovery after Typhoon Morakot in Taiwan. Subwatersheds were defined as “landslide affected” if their landslide ratio in 2009 was larger by at least 0.3% than that in 2008. The 278 landslide-affected subwatersheds were distributed in southern Taiwan (Figure 9). The mean landslide ratio in the 278 landslide-affected subwatersheds in 2009 was larger by 2.86% than that in 2008. The annual landslide recovery rates of the landslide-affected subwatersheds from 2010 to 2017 are shown in Figure 9. The landslide recovery rate of 278 landslide-affected subwatersheds in the first to second years after Typhoon Morakot was 31.6%, and that in the sixth to eighth years was 47.7%. The recovery rate of landslides induced by extreme rainfall events in Taiwan was larger than that of landslides induced by large-scale earthquake events in the world [10,42]. The landslide recovery rate of the subwatersheds with a landslide ratio >3.0% in 2009 was larger than that of all landslide-affected subwatersheds. By contrast, the landslide recovery rate of the subwatersheds with a landslide ratio <3.0% in 2009 was lower than that of all landslide-affected subwatersheds. Furthermore, the landslide recovery rate of the subwatersheds with a landslide ratio >3.0% in 2009 in the first two years after Typhoon Morakot was 35.4%, and that in the sixth to eighth years was 53.7%. The trend of the landslide recovery rate increased after Typhoon Morakot, but the landslide recovery rates in 2013, 2016, and 2017 showed a declining trend.

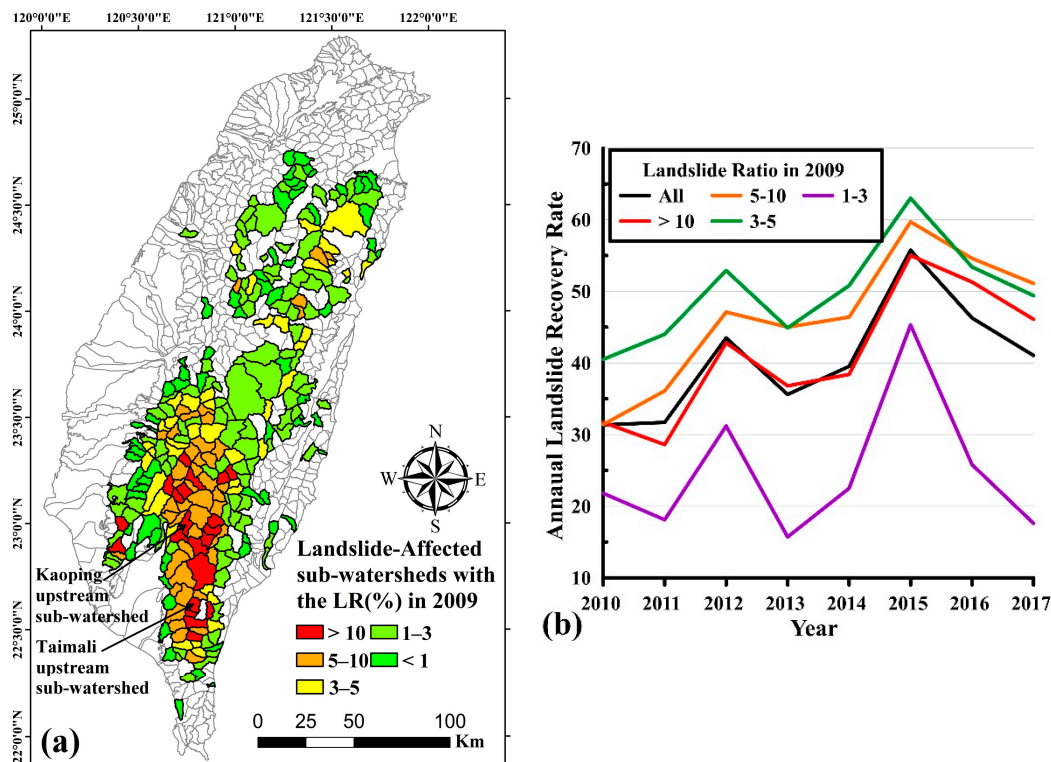


Figure 9. Distribution (a) and the annual landslide recovery rate (b) of 278 landslide-affected sub-watersheds after the 2009 Typhoon Morakot in Taiwan.

Two subwatersheds, namely the Taimali upstream subwatershed and the Kaoping upstream subwatershed (Figure 9a), were selected as examples to assess the spatial distribution of landslide recovery after Typhoon Morakot in 2009. The number of landslides and landslide ratios after Typhoon Morakot in the Taimali upstream subwatershed were 353 and 24.5%, respectively, and those in the Kaoping upstream watershed were 165 and 15.9%, respectively. The Taimali upstream subwatershed and Kaoping upstream subwatershed were listed among the top five subwatersheds with the most severe landslide disasters after Typhoon Morakot in Taiwan. Landslide frequency [9] was defined as the total number of landslides that occurred from 2010 to 2017 in the study. The distribution of landslide frequency in the two subwatersheds from 2010 to 2017 is presented in Figure 10. The mean frequency of landslides in the Taimali and Kaoping upstream subwatersheds induced by Typhoon Morakot was 4.32 and 1.58 years, respectively, and outside the landslide area was 2.24 and 2.41 years, respectively. This result indicates that the landslide recovery time inside the area of the landslide induced by Typhoon Morakot was longer than that outside the landslide area (i.e., the new or enlarged landslide area from 2010 to 2017). Most areas with a high landslide frequency, especially for large-scale landslides, were located in the source area of the landslide induced by Typhoon Morakot. Landslides induced by Typhoon Morakot in the Taimali and Kaoping upstream watersheds accounted for 96.9% and 73.5% of the high landslide frequency grids (i.e., landslide frequency > 5), respectively, inside the landslide area. Moreover, landslides induced by Typhoon Morakot in the Taimali and Kaoping upstream watersheds accounted for 69.2% and 58.9%, respectively, of the low landslide frequency grid (i.e., landslide frequency < 3) inside the landslide area. The grid with a landslide frequency value outside the area of the landslide induced by Typhoon Morakot covered the bank area of sinuous reaches, gully areas, and the boundary of the original landslide area. This result indicated that the area along the sediment transport path was the main region of occurrence of secondary geohazards after extreme rainfall-induced landslide events.

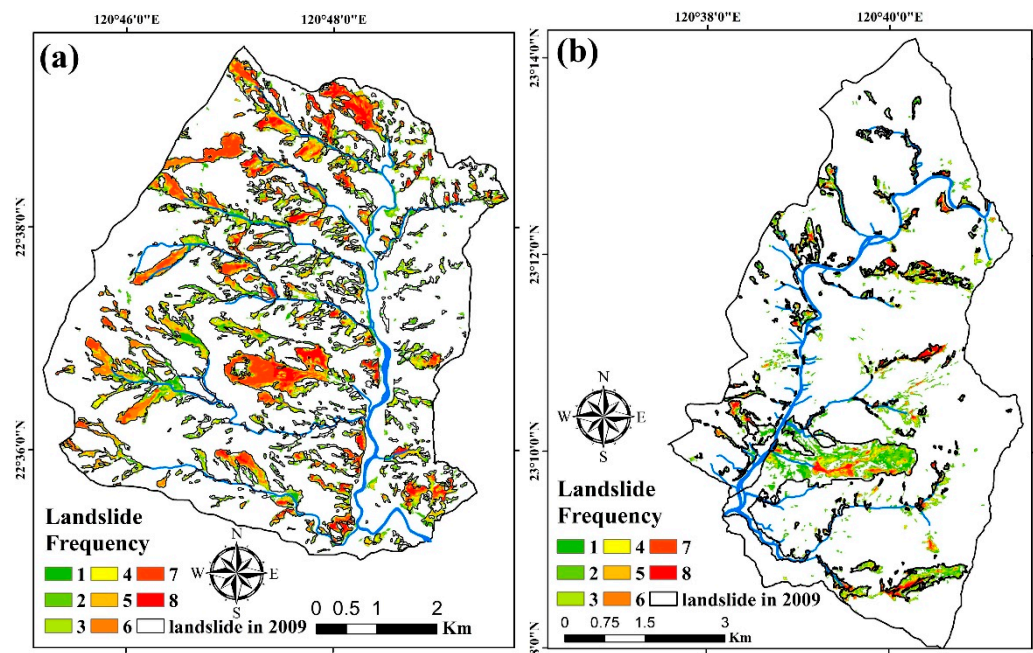


Figure 10. Distribution of landslide frequency from 2010 to 2017 in the Taimali upstream sub-watershed (a) and Kaoping upstream sub-watershed (b).

The recovery of most of the subwatersheds with a landslide ratio $>5\%$ in 2009 in southern Taiwan was difficult in the landslide hillslope, and this was related to four factors, namely landslide-prone geological settings, abundant rainfall during Typhoon Morakot, temporal nonuniform monthly rainfall, and sediment yielded from numerous landslides being deposited on the landslide hillslope or transported to the rivers. Most of the subwatersheds with a landslide ratio of $>5\%$ in 2009 were located in the Lushan Formation, Histsun Formation, Hsinkao Formation, and Sanshia Group and its equivalents (Figure 2). The aforementioned three sediment formations contain shale, sandstone, and slate and are prone to landslides. During Typhoon Morakot in southern Taiwan, the rainfall total was estimated to be >2000 mm in 3 days [3]. The abundant rainfall at these landslide-prone geological formations may have resulted in a severe landslide disaster in 2009 in southern Taiwan, and huge amounts of sediment from this landslide area were deposited on the landslide hillslope or transported to creeks or rivers. This observation can be verified by the finding that the core areas of large-scale landslide cases or the vicinity of creeks or rivers had high landslide frequencies in 2010–2017 (Figure 10). The RSI values at the rainfall stations for the subwatersheds with a landslide ratio $>5\%$ in 2009 (Figure 9a) were >0.70 in 2010–2017, which indicated that most of the rainfall occurred in the rainy season. The seasonal rainfall regime also affects the stability of sediment in southern Taiwan. The sediment in these areas was unstable, and rainfall events with low accumulated rainfall could induce landslides on the hillslope or transport sediment to the rivers. Therefore, the core areas and boundaries of large-scale landslides and the vicinity of creeks and rivers had high landslide frequencies. This was also why the consecutive and intensifying pattern of spatiotemporal landslide hot spots was observed in southern Taiwan. The spatiotemporal analysis of landslide evolution helped characterize the patterns of landslide hot spots and revealed the reason for the difficult and slow recovery after landslides in these regions.

The composition change of soil grain before and after the 2009 Typhoon Morakot in the upstream watershed was also obvious. Most sediment yield from landslides during 2009 Typhoon Morakot was deposited in the down hillslope or transported into the rivers in the upstream watersheds. However, the fine sediment in the sediment deposition in the down hillslope or in the riverbed was gradually transported downstream after several heavy or flooding events after the 2009 Typhoon Morakot [43]. The composition of sediment

deposition in the down hillslope or in the river became coarse. The coarse sediment deposition in the river also became an armor layer.

The mechanisms and triggering factors of secondary geological hazard, and the characteristics of long-term evolution can be explored by using the spatiotemporal hot spot analysis method based on the results in this study. The findings in this study can be referred to or used in other countries that had faced a serious landslide disaster in the past few years, such as the serious landslide disaster caused by heavy rainfall events in July 2020 in southern Japan, including Kumamoto, Nagano, and Kagoshima Prefectures.

The main reasons for the dense landslide caused by the 2009 Typhoon Morakot in Taiwan were extreme rainfall and subsequent flooding. Besides designing engineering to reduce or prevent secondary geological hazards, it is also important to reduce the flooding impact caused by extreme rainfall events in Taiwan [43,44]. Planning flood detention ponds and increasing the riverbed roughness coefficient have been proven to lower the impact of flooding on the safety of human life and property [45,46]. It is also important to examine the drainage ability of each reach or river in the upstream watershed in Taiwan under possible climate change conditions [47].

6. Conclusions

The study period (1990 to 2020) recorded the highest landslide density in the history of Taiwan. The Chi-Chi earthquake in 1999 and several extreme rainfall events resulted in severe landslide disaster events in Taiwan. Therefore, investigating the long-term evolution of landslides and secondary geological disasters is valuable. Based on the analysis using long-term rainfall records and annual landslide inventories for 2003–2017, recovery after landslides was the most difficult in the central mountainous region and southern Taiwan. These regions were also the densest landslide areas during Typhoon Morakot in 2009. The monthly rainfall regimes in the central mountainous region and southern Taiwan are obviously seasonal, making the sediment in these areas unstable. The Mann–Kendall trend test indicated that half of the subwatersheds that exhibited an upward trend of landslide evolution in 2003–2017 were concentrated in the central mountainous region and southern Taiwan. Furthermore, the subwatersheds with the high–high landslide cluster type were also located in the central mountainous region and southern Taiwan based on the spatial cluster and outlier analyses. The main patterns of spatiotemporal landslide hot spots in the central mountainous region and southern Taiwan were consecutive and intensifying. A comparison of landslide recovery rates between regions with large-scale earthquake-induced landslides and extreme rainfall-induced landslides showed that the recovery rate of regions affected by extreme rainfall-induced landslides in Taiwan was higher than that of regions affected by large-scale earthquake-induced landslides in the world. Rainfall-induced landslides were widely distributed in unstable areas of the central mountainous region and southern Taiwan during Typhoon Morakot in 2009 and gradually moved to the core and boundaries of large-scale landslide hillslopes and the vicinity of creeks and rivers.

Supplementary Materials: The following supporting information can be downloaded at: <https://www.mdpi.com/article/10.3390/w15071355/s1>. References [48,49] are cited in the Supplementary Materials.

Funding: This research was funded by the Ministry of Science and Technology of Taiwan (R.O.C.), grant number MOST 111-2625-M-035-001.

Data Availability Statement: Data sharing not applicable. Most data used in the study can be downloaded from <https://data.gov.tw/>.

Conflicts of Interest: The authors declare no conflict of interest.

References

1. Fowler, H.J.; Ali, H. Analysis of extreme rainfall events under the climatic change. In *Rainfall Modeling, Measurement and Applications*; Morbidelli, R., Ed.; Elsevier: Amsterdam, The Netherlands, 2022; pp. 307–326.
2. Panagoulia, D.; Bárdossy, A.; Lourmas, G. Diagnostic statistics of daily rainfall variability in an evolving climate. *Adv. Geosci.* **2006**, *7*, 349–354. [[CrossRef](#)]
3. Panagoulia, D.; Dimou, G. Sensitivity of flood events to global climate change. *J. Hydrol.* **1997**, *191*, 208–222. [[CrossRef](#)]
4. Cheng, J.D.; Huang, Y.C.; Wu, H.L.; Yeh, J.L.; Chang, C.H. Hydrometeorological and landuse attributes of debris flows and debris floods during typhoon Toraji, July 29–30, 2001 in central Taiwan. *J. Hydrol.* **2005**, *306*, 161–173. [[CrossRef](#)]
5. Milliman, J.D.; Lee, T.Y.; Huang, J.C.; Kao, S.J. Impact of catastrophic events on small mountainous rivers: Temporal and spatial variations in suspended- and dissolved-solid fluxes along the Choshui River, central western Taiwan, during typhoon Mindulle, July 2–6, 2004. *Geochim. Cosmochim. Acta* **2017**, *205*, 272–294. [[CrossRef](#)]
6. Wu, C.H.; Chen, S.C.; Chou, H.T. Geomorphologic characteristics of catastrophic landslides during typhoon Morakot in the Kaoping Watershed, Taiwan. *Eng. Geol.* **2011**, *123*, 13–21. [[CrossRef](#)]
7. Wu, C.H.; Chen, S.C.; Feng, Z.Y. Formation, failure, and consequences of the Xiaolin landslide dam, triggered by extreme rainfall from Typhoon Morakot, Taiwan. *Landslides* **2014**, *11*, 357–367. [[CrossRef](#)]
8. Wu, C.; Lin, C. Spatiotemporal hotspots and decadal evolution of extreme rainfall-induced landslides: Case studies in southern Taiwan. *Water* **2021**, *13*, 2090. [[CrossRef](#)]
9. Wu, C.H. Evaluating the landslide stability and vegetation recovery: Case studies in the Tsengwen reservoir watershed in Taiwan. *Water* **2021**, *13*, 3479. [[CrossRef](#)]
10. Shafique, M. Spatial and temporal evolution of co-seismic landslides after the 2005 Kashmir earthquake. *Geomorphology* **2020**, *362*, 107228. [[CrossRef](#)]
11. Yang, W.; Qi, W.; Wang, M.; Zhang, J.; Zhang, Y. Spatial and temporal analyses of post-seismic landslide changes near the epicentre of the Wenchuan earthquake. *Geomorphology* **2017**, *276*, 8–15. [[CrossRef](#)]
12. Rosser, N.; Kinsey, M.; Oven, K.; Densmore, A.; Robinson, T.; Pujara, D.S.; Shrestha, R.; Smutny, J.; Gurung, K.; Lama, S.; et al. Changing significance of landslide Hazard and risk after the 2015 Mw 7.8 Gorkha, Nepal Earthquake. *Prog. Disaster Sci.* **2021**, *10*, 100159. [[CrossRef](#)]
13. Chen, C.W.; Chen, H.; Oguchi, T. Distributions of landslides, vegetation, and related sediment yields during typhoon events in northwestern Taiwan. *Geomorphology* **2016**, *273*, 1–13. [[CrossRef](#)]
14. Qin, S.; Ding, J.; Ge, X.; Wang, J.; Wang, R.; Zou, J.; Tan, J.; Han, L. Spatio-Temporal Changes in Water Use Efficiency and Its Driving Factors in Central Asia (2001–2021). *Remote Sens.* **2023**, *15*, 767. [[CrossRef](#)]
15. Zhao, Z.; Tang, X.; Wang, C.; Cheng, G.; Ma, C.; Wang, H.; Sun, B. Analysis of the Spatial and Temporal Evolution of the GDP in Henan Province Based on Nighttime Light Data. *Remote Sens.* **2023**, *15*, 716. [[CrossRef](#)]
16. Wang, S.; Cui, G.; Li, X.; Liu, Y.; Li, X.; Tong, S.; Zhang, M. GRACE Satellite-Based Analysis of Spatiotemporal Evolution and Driving Factors of Groundwater Storage in the Black Soil Region of Northeast China. *Remote Sens.* **2023**, *15*, 704. [[CrossRef](#)]
17. Aeberli, A.; Phinn, S.; Johansen, K.; Robson, A.; Lamb, D.W. Characterisation of Banana Plant Growth Using High-Spatiotemporal-Resolution Multispectral UAV Imagery. *Remote Sens.* **2023**, *15*, 679. [[CrossRef](#)]
18. Mansour, S.; Ghoneim, E.; El-Kersh, A.; Said, S.; Abdelnaby, S. Spatiotemporal Monitoring of Urban Sprawl in a Coastal City Using GIS-Based Markov Chain and Artificial Neural Network (ANN). *Remote Sens.* **2023**, *15*, 601. [[CrossRef](#)]
19. Chen, M.; Tang, C.; Xiong, J.; Shi, Q.Y.; Li, N.; Gong, L.F.; Wang, X.D.; Tie, Y. The long-term evolution of landslide activity near the epicentral area of the 2008 Wenchuan earthquake in China. *Geomorphology* **2020**, *367*, 107317. [[CrossRef](#)]
20. Tang, C.; Van Westen, C.J.; Tanyas, H.; Jetten, V.G. Analysing post-earthquake landslide activity using multi-temporal landslide inventories near the epicentral area of the 2008 Wenchuan earthquake. *Nat. Hazards Earth Syst. Sci.* **2016**, *16*, 2641–2655. [[CrossRef](#)]
21. Liu, C.C.; Liu, J.G.; Lin, C.W.; Wu, A.M.; Liu, S.-H.; Shieh, C.-L. Image processing of formosat-2 data for monitoring south Asia tsunami. *Int. J. Remote Sens.* **2007**, *28*, 3093–3111. [[CrossRef](#)]
22. Liu, C.C.; Ko, M.H.; Wen, H.L.; Fu, K.L.; Chang, S.-T. Instability Index Derived from a Landslide Inventory for Watershed Stability Assessment and Mapping. *ISPRS Int. J. Geo-Inf.* **2019**, *8*, 145. [[CrossRef](#)]
23. Wu, C. Certainty Factor Analyses and Spatiotemporal Characteristics of Landslide Evolution: Case Studies in the Chishan River Watershed in Taiwan. *ISPRS Int. J. Geo-Inf.* **2022**, *11*, 382. [[CrossRef](#)]
24. Ma, S.; Qiu, H.; Zhu, Y.; Yang, D.; Tang, B.; Wang, D.; Wang, L.; Cao, M. Topographic Changes, Surface Deformation and Movement Process before, during and after a Rotational Landslide. *Remote Sens.* **2023**, *15*, 662. [[CrossRef](#)]
25. Kuang, J.; Ng, A.H.-M.; Ge, L.; Metternicht, G.I.; Clark, S.R. Joint Use of Optical and Radar Remote Sensing Data for Characterizing the 2020 Aniangzhai Landslide Post-Failure Displacement. *Remote Sens.* **2023**, *15*, 369. [[CrossRef](#)]
26. Li, C.; Wang, M.; Liu, K. A decadal evolution of landslides and debris flows after the Wenchuan earthquake. *Geomorphology* **2018**, *323*, 1–12. [[CrossRef](#)]
27. Kinsey, M.E.; Rosser, N.J.; Robinson, T.R.; Densmore, A.L.; Shrestha, R.; Pujara, D.S.; Oven, K.J.; Williams, J.G.; Swirad, Z.M. Evolution of Coseismic and Post-seismic Landsliding After the 2015 Mw 7.8 Gorkha Earthquake, Nepal. *J. Geophys. Res. Earth Surf.* **2021**, *126*, e2020JF005803. [[CrossRef](#)]
28. Roback, K.; Clark, M.K.; West, A.J.; Zekkos, D.; Li, G.; Gallen, S.F.; Chamlagain, D.; Godt, J.W. The size, distribution, and mobility of landslides caused by the 2015 Mw7.8 Gorkha earthquake, Nepal. *Geomorphology* **2018**, *301*, 121–138. [[CrossRef](#)]

29. Zhang, X.; Chen, L.; Zhou, C. Deformation Monitoring and Trend Analysis of Reservoir Bank Landslides by Combining Time-Series InSAR and Hurst Index. *Remote Sens.* **2023**, *15*, 619. [CrossRef]
30. Medhat, N.I.; Yamamoto, M.-Y.; Ichihashi, Y. Incliner and Improved SBAS Methods with a Random Forest for Monitoring Landslides and Anchor Degradation in Otoyo Town, Japan. *Remote Sens.* **2023**, *15*, 441. [CrossRef]
31. Conforti, M.; Mercuri, M.; Borrelli, L. Morphological Changes Detection of a Large Earthflow Using Archived Images, LiDAR-Derived DTMs, and UAV-Based Remote Sensing. *Remote Sens.* **2021**, *13*, 120. [CrossRef]
32. Lin, S.C.; Ke, M.C.; Lo, C.M. Evolution of landslide hotspots in Taiwan. *Landslides* **2017**, *14*, 1491–1501. [CrossRef]
33. Science. A Massive Experiment in Taiwan Aims to Reveal Landslides' Surprising Effect on the Climate. Available online: <https://www.science.org/content/article/massive-experiment-taiwan-aims-reveal-landslides-surprising-effect-climate> (accessed on 25 January 2023).
34. Government Open Data. Available online: <https://data.gov.tw/dataset/140111> (accessed on 24 September 2022).
35. Hydrological Data in Taiwan. Available online: <https://www.wra.gov.tw/cp.aspx?n=3168> (accessed on 24 September 2022).
36. Walsh, R.P.D.; Lawler, D.M. Rainfall seasonality: Description, spatial patterns and change through time. *Weather* **1981**, *36*, 201–208. [CrossRef]
37. Tanyas, H.; Kirschbaum, D.; Görüm, T.; van Westen, C.J.; Tang, C.; Lombardo, L. A closer look at factors governing landslide recovery time in post-seismic periods. *Geomorphology* **2021**, *391*, 107912. [CrossRef]
38. Anselin, L. Local indicators of spatial association-LISA. *Geogr. Anal.* **1995**, *27*, 93–115. [CrossRef]
39. Getis, A.; Ord, J.K. The analysis of spatial association by use of distance statistics. *Geogr. Anal.* **1992**, *24*, 189–206. [CrossRef]
40. ESRI Website. Available online: <https://pro.arcgis.com/en/pro-app/2.8/tool-reference/space-time-pattern-mining/emerginghotspots.htm> (accessed on 24 September 2022).
41. Liu, J.; Mason, P.J.; Bryant, E.C. Regional assessment of geohazard recovery eight years after the Mw7.9 Wenchuan earthquake: A remote-sensing investigation of the Beichuan region. *Int. J. Remote Sens.* **2018**, *39*, 1671–1695. [CrossRef]
42. Tsai, S.R. Spatial Variation of Soil Properties in Kaoping River Basin Prior and Post Typhoon Morakot. Master's Thesis, National Pingtung University of Science and Technology, Taiwan, 2011; p. 52.
43. Lousada, S.; Cabezas, J.; Castanho, R.A.; Gómez, J.M.N. Hydraulic Planning in Insular Urban Territories: The Case of Madeira Is-land—Ribeira Brava. *Water* **2021**, *13*, 2951. [CrossRef]
44. Lousada, S.; Gonçalves, L.; Atmaca, A. Hydraulic Planning in Insular Urban Territories: The Case of Madeira Island—São Vicente. *Water* **2022**, *14*, 112. [CrossRef]
45. Lousada, S.; Castanho, R.A. GIS-Based Assessment of Morphological and Hydrological Parameters of Ribeira Dos Socorridos and Ribeira Do Vigario Basins, Madeira Island, Portugal. *Curr. World Environ.* **2021**, *16*, 408–426. [CrossRef]
46. Lousada, S.A.N.; Moura, A.D.S.; Gonçalves, L.B. Numerical modelling of the flow rate in artificial water channels: Application to Ribeira Brava's stream. *Rev. Bras. Planej. Desenvol.* **2020**, *9*, 39–59. [CrossRef]
47. Lousada, S.; Cabezas, J.; Castanho, R.A.; Gómez, J.M.N. Land-Use Changes in Insular Urban Territories: A Retrospective Analysis from 1990 to 2018. The Case of Madeira Island—Ribeira Brava. *Sustainability* **2022**, *14*, 16839. [CrossRef]
48. Liu, C.-C.; Chen, P.-L. Automatic extraction of ground control regions and orthorectification of formosat-2 imagery. *Opt. Express* **2009**, *17*, 7970–7984. [CrossRef] [PubMed]
49. Liu, C.-C.; Shieh, C.-L.; Wu, C.-A.; Shieh, M.-L. Change detection of gravel mining on riverbeds from the multi-temporal and high-spatial-resolution formosat-2 imagery. *River Res. Appl.* **2009**, *25*, 1136–1152. [CrossRef]

Disclaimer/Publisher's Note: The statements, opinions and data contained in all publications are solely those of the individual author(s) and contributor(s) and not of MDPI and/or the editor(s). MDPI and/or the editor(s) disclaim responsibility for any injury to people or property resulting from any ideas, methods, instructions or products referred to in the content.